High-Performance Organic-Inorganic Hybrid Photodetectors Based on P3HT:CdSe Nanowire Heterojunctions on Rigid and Flexible Substrates

Xianfu Wang, Weifeng Song, Bin Liu, Gui Chen, Di Chen, Chongwu Zhou, and Guozhen Shen**

Organic-inorganic hybrid photoelectric devices draw considerable attention because of their unique features by combining the relatively low ionization potential of the organic molecules and the high electron affinity of inorganic semiconductors. Hybrid organic-inorganic poly(3-hexylthiophene) (P3HT):CdSe nanowire heterojunction photodetectors are first demonstrated on silicon substrates, exhibiting a greatly enhanced photocurrent, a fast response, and a recovery time shorter than 0.1 s. Flexible hybrid photodetectors with excellent mechanical flexibility and stability are also fabricated on both poly(ethylene terephthalate) (PET) substrates and printing paper. The flexible devices are successfully operated under bending up to almost 180° and show an extremely high on/off switching ratio (larger than 500), a fast time response (about 10 ms), and excellent wavelength-dependence, which are very desirable properties for its practical application in high-frequency or high-speed flexible electronic devices.

1. Introduction

Photoconductivity is a well-known property of semiconductors, which implies the electrical conductivity changes due to incident radiation. Photodetection in the visible-light or UV region shows extensive applications including environmental and biological research, optical communication, sensors, and missile-launch detection.[1] Several types of photodetectors[2–11] have been developed up to now, among which organic-inorganic hybrid photodetectors have drawn considerable attention in recent years.[12–15] Compared with other types of photodetectors, organic-inorganic hybrid photodetectors have unique features, taking advantage of both the superior intrinsic carrier mobilities and the broad-band absorption of inorganic based devices, as well as easy-formation properties, excellent mechanical flexibility, and tunable functionality through modification of the structures of the molecules or the monomers, of the polymers of the organic based devices. At the same time, on the other hand, they overcome their own shortcomings.[16–18] Different prototypes of hybrid photodetectors have been constructed and tested for their photoelectric properties. For example, polymers in conjunction with different inorganic components such as $CuInSe_2$,[14] TiO_2,[19] ZnO,[20] Ge,[15] and $Cu_2ZnSnSe_4$[21] have been developed as promising photoelectric devices. However, all of the reported hybrid photodetectors have used either nanoparticles or quantum dots as the inorganic component, but hybrid photodetectors with 1D semiconductor nanostructures as the inorganic component haven't yet been reported.[22] Thus, it is highly desired to design high-performance organic-inorganic hybrid photodetectors by using 1D inorganic semiconductor nanostructures since 1D nanostructures represent the smallest dimensions for efficient transport of electrons and excitons and thus are ideal building blocks for nanoscale electronic and optoelectronic devices.

Flexible devices have attracted extensive attention for their potential applications in future paper displays, wearable devices, and energy-storage devices,[23–26] owing to their attractive properties, including biocompatibility, flexibility, light weight, shock resistance, softness, and transparency.[27] Recently, flexible photodetectors have become one of the focuses of current research because they may be fit for some unique applications in various new areas (e.g., portable devices, aerospace science, and civil engineering) that require flexible, lightweight, and mechanical shock-resistive sensing elements.[28] In this paper, by utilizing P3HT and CdSe nanowires (NWs) as the components, we fabricated hybrid photodetectors on a rigid substrate and flexible substrates (both PET and printing paper) with superior performance. P3HT was selected because it is a classical π-electron conjugated polymer with a high hole-transport rate and strong absorption in the visible range,[29] while CdSe NWs are used as an electron-transport material with a high electrical conductivity because of their high surface-to-volume ratio, significant increased surface area, and controllable surface charge.[30–37] Furthermore, CdSe and P3HT have complementary absorption

X. F. Wang, W. F. Song, B. Liu, G. Chen, Prof. D. Chen, Prof. G. Z. Shen
Wuhan National Laboratory for Optoelectronics (WNLO)
Huazhong University of Science and Technology (HUST)
Wuhan, 430074, China
E-mail: gzshen@mail.hust.edu.cn
Prof. C. W. Zhou
Department of Electrical Engineering
University of Southern California
Los Angeles CA 90089
E-mail: chongwuz@usc.edu

DOI: 10.1002/adfm.201201786

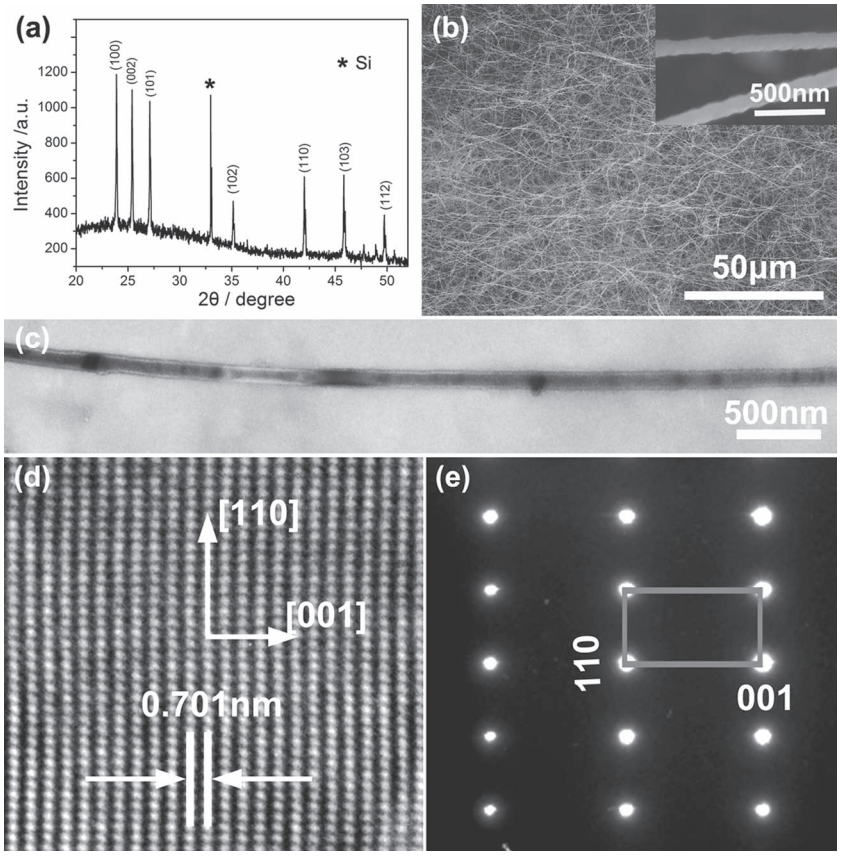

Figure 1. a) XRD pattern, b) SEM images, c) TEM image, d) HR-TEM image and e) SAED pattern of the as-prepared CdSe nanowires.

spectra in the visible spectrum,[38] which plays a key role in improving the sensitivity of the hybrid devices. The as-fabricated hybrid photodetectors on flexible substrates showed high flexibility, good folding strength, and excellent wavelength-dependence and electrical stability. Moreover, the fast response characteristics to high-frequency light signals make such flexible hybrid photodetectors desirable for future practical application in high-frequency or high-speed devices.

2. Results and Discussion

2.1. Synthesis and Structural Analysis

Single-crystalline CdSe NWs were synthesized by a thermal-evaporation method using CdSe powders as the source and gold nanoparticles as the catalysts. The crystalline phase of the product and its crystallographic orientation were identified by X-ray diffraction (XRD) studies, as shown in **Figure 1**a. All of the peaks, except the peak marked with the asterisk (coming from the silicon substrate), can be indexed to CdSe with a hexagonal phase (JCPDS: 65–3415), indicating the formation of a pure CdSe product. Figure 1b shows a general scanning electron microscopy (SEM) image of the as-synthesized CdSe nanostructures, revealing the formation of 1-D wire-like materials with a length of hundreds of micrometers on a large scale. A higher-magnification SEM image is shown in the Figure 1b inset, where the NWs were found to have uniform diameters of 100 nm. To get more information of the obtained CdSe NWs, transmission electron microscopy (TEM) was further performed. A typical TEM image of a single CdSe NW shown in Figure 1c indicates that the nanowire has a uniform diameter (≈100 nm) along its entire length. The high-resolution TEM (HR-TEM) image (Figure 1d) and the corresponding selected-area electron diffraction (SAED) pattern (Figure 1e) reveal that the CdSe NWs were hexagonal single crystals grown along the [001] orientation.

2.2. Photodetectors Based on Rigid Substrates

To fabricate hybrid photodetectors, the CdSe NWs were first mixed with P3HT to form a hybrid film on a SiO_2 (300 nm)/Si wafer (shown in Supporting Information, Figure S1). A prototype photodetector was then constructed by depositing silver electrodes

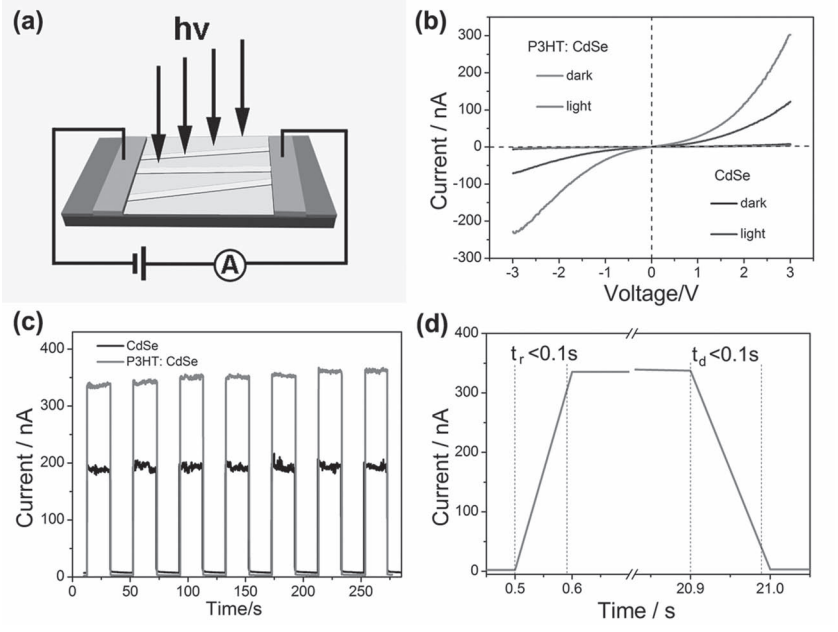

Figure 2. a) Schematic illustration, b) *I–V* characteristics, c) reproducible on/off switching; and d) response time/recovery time of the P3HT:CdSe NW hybrid photodetector on the silicon substrate.

to investigate its photoresponse to visible-light irradiation. A schematic illustration of the hybrid device is shown in **Figure 2**a, consisting of the hybrid film, silver electrodes, and the SiO_2/Si substrate. Figure 2b shows the *I–V* curves of the devices exposed to white light and under dark conditions. For the hybrid photodetectors, a high photoexcited current of 320 nA was recorded at a low bias of 3.0 V, while only 120 nA was reached for the pure CdSe NWs devices. The corresponding logarithmic relationship between the current and voltage is replotted in Figure S2 in the Supporting Information. Figure 2c shows the photocurrent of the hybrid devices during repetitive switching of light illumination, or on/off switching. It should be noted that the hybrid photodetector showed an outstanding stability. No obvious degradation was observed during scores of cycles. The high sensitivity and stability of the hybrid devices is promising for large-area photodetector applications.

In Figure 2c, the photocurrent increased and decreased as a response to the on/off states by periodically turning the light on and off with a power of 140 mW cm^{-2} at a bias of 3.0 V. The switching in the two states was very fast and reversible, allowing the device to act as a high-quality photosensitive switch. For the hybrid photodetectors, the current was only 2.5 nA in the dark. However, at an incident light intensity of 140 mW cm^{-2} and a bias voltage of 3.0 V, the current could approach 350 nA, giving an on/off ratio of 140. In contrast, devices based on pure CdSe NWs showed quite a low photocurrent of 190 nA at a bias voltage of 3.0 V, an enhancement of about 25 times compared with the dark current of 7.5 nA. In the case of devices made from pure P3HT, the photocurrent after illumination was relatively low (about 5.1 nA) and the on/off ratio was lower than 2 (see **Figure 3**a), consistent with previously reported results.[39] Notably, the dark current in the hybrid device (2.5 nA) at a bias voltage of 3.0 V was lower than that of pure CdSe NWs (7.5 nA) or P3HT (3.6 nA) at the same bias, which could be attributed to difficult charge transportation through the interface of the P3HT and the CdSe NWs without light illumination. The result is in agreement with a previously reported hybrid photodetector with $CuInSe_2$ nanoparticles and aP3HT in a hybrid film.[14] The rise time and decay time, defined as the time taken for the initial current to increase to 90% of the peak value, or vice versa, are measured to be shorter than 0.1 s, as shown in Figure 2d.

The high photosensitivity of the hybrid devices was further confirmed by photocurrent measurements on the devices at different incident light densities and the photodetectors showed good intensity-dependent properties, as shown in Figure 3b, and Figure S3 and S4 in the Supporting Information. When the intensity of the incident light was changed, the photocurrent of the devices remarkably changed accordingly, which can be attributed to a change in the photon intensity of the hybrid organic-inorganic devices. Light can be absorbed through the whole thickness of the device and that of both types of charge carrier run within the device. These results prove the promising potential of the hybrid devices as a photoswitch and a highly photosensitive detector.

In order to explore the reason for the enhanced photoresponse effect, we measured the UV–vis absorption spectra of a pure CdSe NW film, a P3HT film, and a P3HT:CdSe NW hybrid film, as shown in **Figure 4**. The CdSe NW film shows a wide absorption spectrum in the range of 340 nm to 700 nm

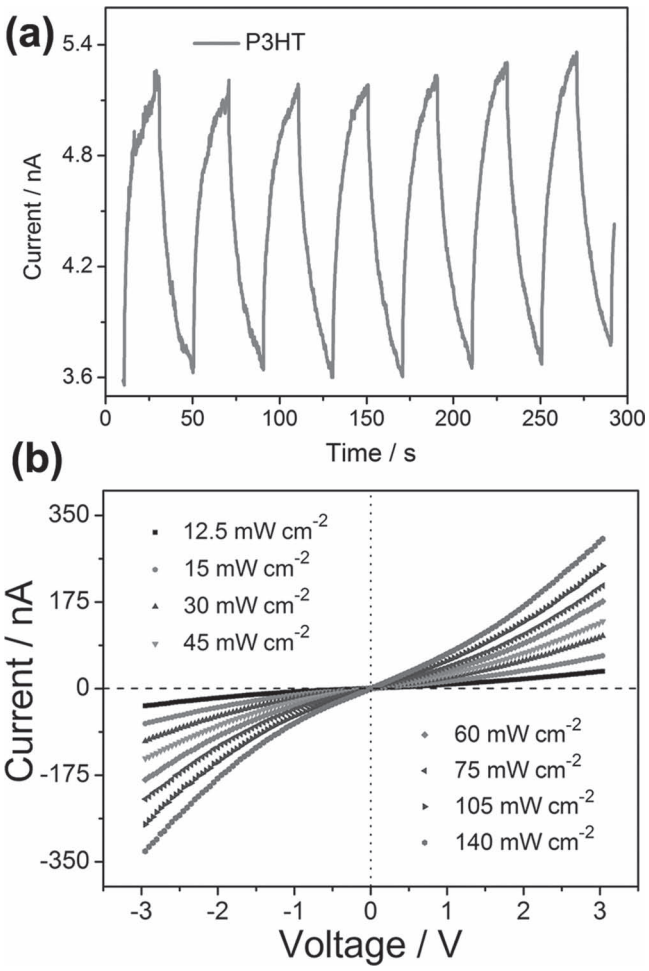

Figure 3. a) On/off switching of a device made from a pure P3HT film at an incident light density of 140 mW cm^{-2} and a bias voltage of 3.0 V. b) *I–V* characteristics of the hybrid photodetector as a function of light intensity ranging from 12.5 mW cm^{-2} to 140 mW cm^{-2}.

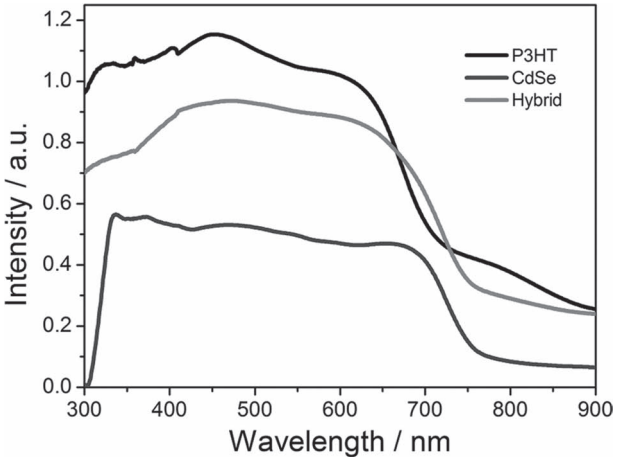

Figure 4. a) UV–vis absorption spectra of P3HT film, CdSe NW film, and P3HT:CdSe NW hybrid film (≈3:5 weight ratio).

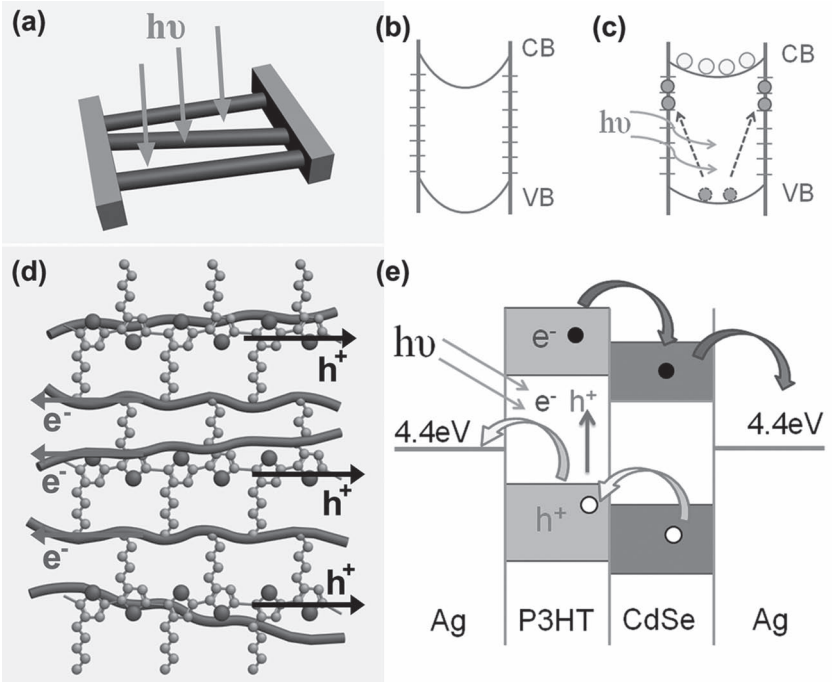

Figure 5. a) Schematic of the CdSe NW film photodetector. b,c) Schematic illustration of the energy-band diagrams of CdSe NWs in the dark (b), and under light illumination (c). d) A schematic of the P3HT:CdSe NW hybrid film. e) Energy level diagram for P3HT and CdSe NWs under illumination, illustrating CdSe NWs are used as the electron-transport material, whereas P3HT is an effective hole-transport material.

and a quite low absorption at wavelengths longer than 700 nm. While the spectrum of the P3HT film shows a characteristic wide peak in the range of 300–650 nm, the absorption spectrum of the P3HT:CdSe NW film exhibits a stronger absorption at wavelengths of 300–700 nm, as well as a significant absorption at wavelengths longer than 750 nm. The result indicates that the inlay of CdSe NWs into the P3HT film significantly broadened the absorption spectrum, and it is believed that the synergy effect contributed greatly to the enhanced photoresponse of the hybrid films.

Because of the high surface-to-volume ratio, trapping at surface states drastically affects the transport and photoconduction properties of the semiconducting nanowires.[40] **Figure 5**a–c show a schematic illustration of the photoconduction mechanism in the presence of a high intensity of hole-trap states at the CdSe NWs surfaces. Upon illumination with a photoenergy larger than the semiconductor band gap (E_g), electron-hole pairs are photogenerated and holes are readily trapped at the surface, leaving unpaired electrons behind, which increases the conductivity of the CdSe NWs under an applied electric field (Figure 5a). Schematics of the energy-band diagrams of the CdSe NWs in the dark and under illumination are displayed in Figure 5b and 5c, respectively, illustrating the charge-separation process of photogenerated electrons and holes under the intrinsic electric field of the NWs and the occupation of the states by photogenerated holes. For the hybrid photodetector, despite trapping at the surface of the CdSe NWs, the interface of the P3HT:CdSe NW hybrid film plays another key role in charge dissociation and transportation. Exciton dissociation is well known to occur efficiently at the interface of two semiconductors mixed together in a blend film, such as a conjugated polymer and a fullerene derivative.[18,39,41] The photoexcited electrons can be accepted by the material with the higher electron affinity, while the holes can be caught by the material with the relatively lower ionization potential.[18,39,41] In our hybrid system, the CdSe NWs were combined with conjugated P3HT to create a charge-transfer junction with a large interfacial area (Figure 5d). From the schematic energy-level diagram of the CdSe NWs and P3HT, it can be seen that the CdSe NWs are used as the electron-transport material, whereas P3HT is an effective hole-transport material in its regioregular form, demonstrating the highest photocurrent observed in hybrid photodetectors (Figure 5e). In addition, in the hybrid film, the CdSe NWs are

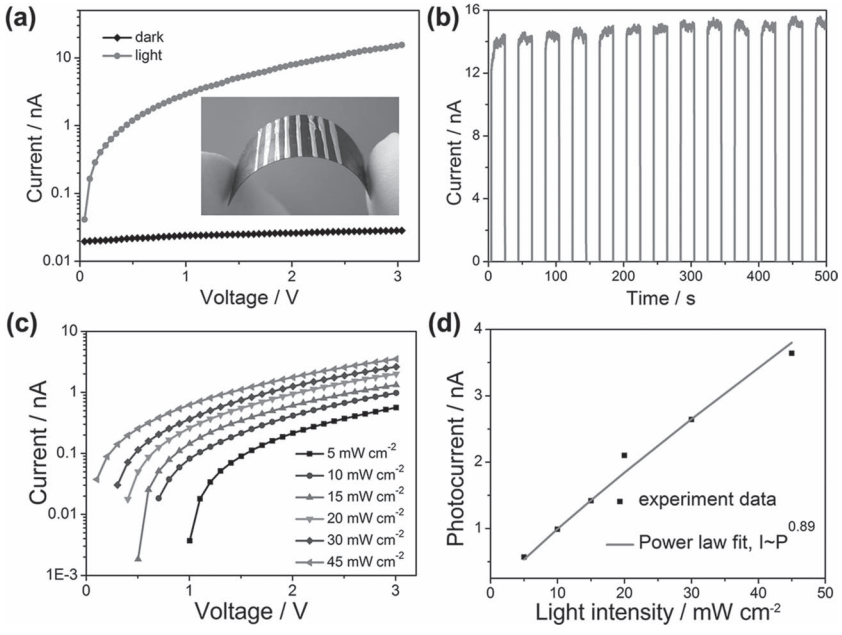

Figure 6. a) *I–V* characteristics of the hybrid film photodetector on a PET substrate illuminated with and without a white light, respectively. The inset is a typical optical image of the hybrid photodetector under bending. b) The reproducible on/off switching of the flexible hybrid film photodetector. c) *I–V* curves of the flexible hybrid photodetector under white-light irradiation with different light intensities. d) Photocurrent as a function of light intensity and the corresponding fitting curve using the power law.

highly dispersed in the P3HT matrix, resulting in the formation of a 3D interconnected network. Such a structure leads to a large interface area for charge separation. Therefore, long-lived charge separation and good transport might be achieved in the hybrid device. All of the above effects resulted in a greatly enhanced photoresponse of the hybrid devices over that of the single-component devices.

2.3. Flexible Hybrid Photodetectors

The fabrication of flexible electronic and optoelectronic devices on plastic substrates has attracted considerable attention owing to the proliferation of handheld, portable consumer electronics.[42] In order to study the flexibility and photoresponse of the P3HT and the CdSe NW hybrid films, we prepared hybrid photodetectors on PET substrates. The inset in **Figure 6**a is a photograph of an as-fabricated flexible hybrid photodetector, showing excellent flexibility. The *I–V* characteristics of the hybrid photodetectors in the dark and under light illumination are shown in Figure 6a and Figure S5 in the Supporting Information, respectively. The *I–V* curve displays a non-linear behavior, which might be attributed to the Schottky barrier at the metal-semiconductor contacts.[43] A great enhancement of the device current was clearly observed when the device was illuminated using white light with an intensity of 140 mW cm^{-2}. In the dark, the device was nearly insulating, with a dark current of 30 pA at a fixed voltage of 3.0 V, while, upon illumination, the current increased immediately and the value approaches 16 nA at an incident-light intensity of 140 mW cm^{-2}. The on/off switching ratio is thus larger than 500. Figure 6b presents the time-dependent photoresponse of the hybrid photodetector measured by periodically turning the white light on and off at a bias of 3.0 V. Upon illumination, the photocurrent rapidly increased to a stable state, and then drastically decreased to its initial level when the light was turned off. The performance of the device placed in air for two weeks still remained unchanged, indicating the excellent stability and reproducible characteristics of the flexible hybrid photodetectors.

To demonstrate the excellent photoresponse characteristics of the flexible hybrid photodetector, we also explored the photosensitivity dependence on light intensity. Figure 6c and Figure S6 in the Supporting Information show the *I–V* curves of the flexible device when illuminated with light at different intensities. The photocurrent was found to increase with increasing light intensity, consistent with the fact that the charge-carrier photogeneration efficiency is proportional to the absorbed photon flux. The corresponding light-intensity dependence of the photocurrent is plotted in Figure 6d, which can be fitted to a power law, $I_p \approx P^{\theta}$, where θ determines the response of the photocurrent to light intensity. The fitting shows a nearly linear behavior with $\theta = 0.89$. According to previous reports, a non-unity ($0.5 < \theta < 1$) exponent suggests a complex process of electron-hole generation, recombination, and trapping within a semiconductor.[44]

The flexible hybrid photodetectors also showed excellent wavelength (λ)-dependent characteristics. **Figure 7**a and Figure S7 in the Supporting Information show the *I–V*

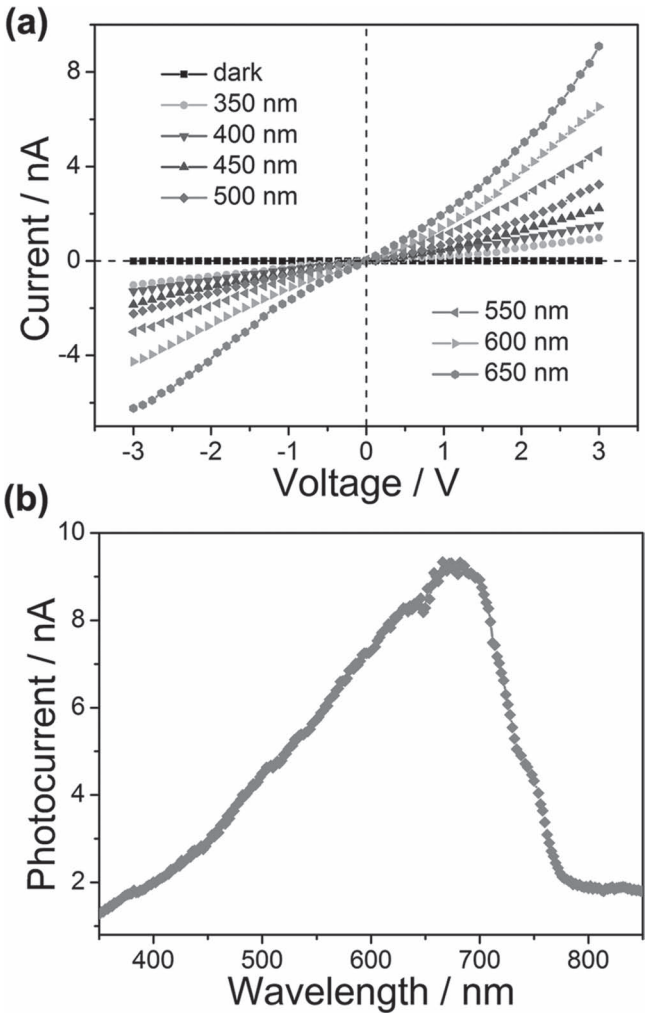

Figure 7. a) The *I–V* characteristics of the flexible hybrid devices illuminated with light at different wavelengths. b) A spectroscopic photoresponse of the flexible device to light with different wavelengths.

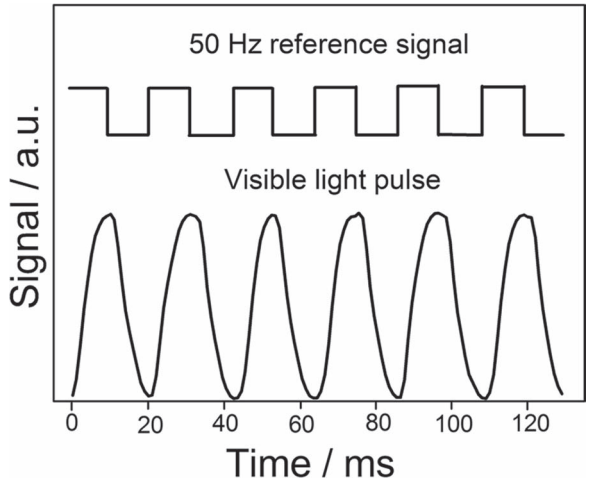

Figure 8. A transient response by illuminating the flexible P3HT:CdSe NW hybrid film photodetector with the white light, pulse chopped at a frequency of 50 Hz with reference signal.

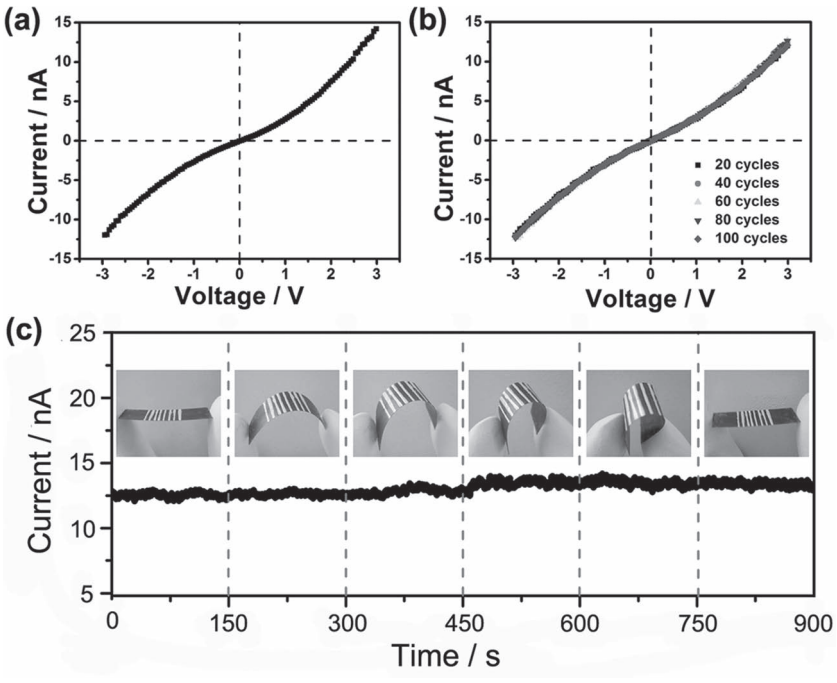

Figure 9. *I–V* curves of the flexible hybrid photodetector under white-light illumination without bending (a), and after 20, 40, 60, 80, and 100 cycles of bending (b). c) The *I–t* curve of the flexible hybrid photodetector when bent with different curvatures under a bias voltage of 3.0 V. The inserts are corresponding photographs of the device under the different bending states.

characteristics of the flexible hybrid devices when illuminated with light of different wavelengths. The light intensity was fixed at 2.5 mW cm^{-2}. For comparison, the *I–V* curve of the devices under dark conditions is also shown in the Figure. As can be seen from the curves, the photocurrent increased gradually as the light wavelength increased from 350 nm to 650 nm, and then decreased as the light wavelength increased from 700 nm to 850 nm. It is clearly revealed that the photoconductance ($G = I/V$) is highly sensitive to the excitation wavelength. From the *I–V* results, the photoconductance was calculated to be 3.03 nS at 650 nm and 2.9 nS at 700 nm, while the value decreased quickly to 0.59 nS at 800 nm, and eventually to 0.00032 nS in a dark state. A cutoff wavelength of about 760 nm and a fairly low response for a wavelength longer than 760 nm are observed in Figure 7b, which is in good agreement with the absorption spectrum of the P3HT:CdSe NW hybrid film (Figure 4). The slight increase of the photoresponse on the long-wavelength side is possibly due to the transition of carriers from the defect states in the bandgap to the conduction band, while the drop of the response on the shorter wavelength side is attributed to the enhanced absorption of high-energy photons at or near the surface region of the hybrid semiconductor.[5]

The time response speed is usually a key factor for sensing performance and it determines the capability of a photodetector to follow a fast-varying optical signal. The P3HT:CdSe NW hybrid film also exhibits fast response characteristics to high-frequency light signals. Under a white-light source pulse chopped at a frequency of 50 Hz, as shown in **Figure 8**. We found that both the rise and the decay times were measured to be on the millisecond timescale (about 10 ms). Such a fast response is very desirable for its practical application in high-frequency or high-speed devices, such as light-wave communications or optoelectronic switches.[45]

In order to br fit for real applications, the electrical properties of the of flexible electronic devices under bending should remain unchanged. **Figure 9**a,b show the *I–V* curves of the flexible hybrid devices after bending for different cycles, in order to evaluate the folding endurance. From the curves, it can be seen that, compared with the conductance of the flexible hybrid device without bending (Figure 9a), the conductance endurance of the device remained almost constant after 20, 40, 60, 80, and 100 cycles of bending (Figure 9b). We also checked the current flow through the device at six different curvatures, which can be clearly seen from the corresponding photographs inset in Figure 9c. The corresponding *I–t* curve of the flexible hybrid device under different bending states is shown in Figure 9c. Clearly, the current was nearly unchanged in the different bending states, revealing that the conductance of the P3HT:CdSe NW hybrid film is hardly affected by the external bending stress. These results indicate the high flexibility, good folding strength, and electrical stability of the hybrid photodetectors.

Moreover, we also fabricated flexible hybrid photodetectors on highly flexible printing paper, also showing excellent performance, as can be seen from **Figure 10**. A photograph of the hybrid photodetector rolled into a cylinder in Figure 10a illustrates the outstanding mechanical flexibility. The reproducible on/off switching of the flexible photodetectors in Figure 10b further demonstrates the superiority of the organic-inorganic hybrid photodetector.

3. Conclusions

In conclusion, organic-inorganic hybrid photodetectors based on P3HT:CdSe NW film were first fabricated on rigid substrates. Compared with photodevices fabricated by using only CdSe NW and P3HT films, the hybrid photodetector showed an enhanced photoresponse and stability because of the high hole-transport rate of P3HT, the high electrical conductivity of CdSe NWs, and the synergy absorption spectra in the visible spectrum of the components. Flexible hybrid photodetectors constructed on PET and printing paper were also investigated, exhibiting high flexibility, good folding strength, excellent wavelength-dependent electrical stability and a very fast response to high-frequency light signals, which are very desirable for its practical application in high-frequency or high-speed flexible electric devices. Flexible photodetectors may have potential application in large-scale photosensors, flexible solar cells, lightweight tracking-and-guidance devices, folding automatic control systems, fiber-optical sensors, and so on.

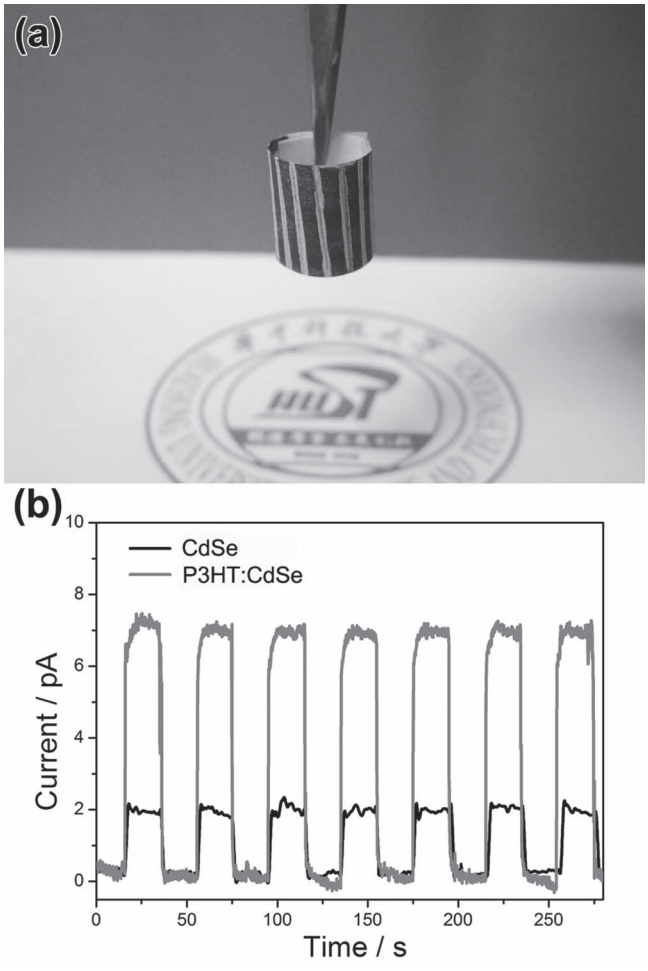

Figure 10. a) Photograph of the hybrid photodetector on a printing paper. b) The reproducible on/off switching of the photodetectors based on a flexible hybrid film and a pure CdSe NW film upon white-light (140 mW cm^{-2}) illumination.

4. Experimental Section

Synthesis and Characterization of CdSe NWs: Single-crystalline CdSe NWs were synthesized in a furnace with a horizontal quartz tube with a 30 mm inner diameter and a length of 800 mm. In a typical process, commercially available CdSe powder (Alfa Aesar, 99.9995% purity), serving as the source material, was placed in the center of the quartz tube, which was inserted in a horizontal tube furnace. Si (100) substrate with a 10 nm Au thin film was then placed downstream, about 10 cm away from the CdSe powder to collect the product. The quartz tube was first pumped down to 600 Torr, and then the system was heated from room temperature to 800 °C over 30 min. This system was kept at this temperature for 90 min after the tube had been purged with pure N_2 for 30 min. During the whole process, a N_2 flow of 100 sccm was introduced into the reaction system. After the reaction, the product was obtained on the substrate for characterization by X-ray diffraction (XRD) using an X'pert Pro diffractometer. The morphology and microstructures were checked using SEM (Sirion 200), TEM (Philips CM 20), and HR-TEM (Philips CM 200).

Fabrication of Hybrid Photodetectors: P3HT (30 mg) was first dissolved in 2 mL of toluene. A solution of the CdSe NWs (100 µL, ≈50 mg mL^{-1}) and a P3HT solution (200 µL) were mixed to form the final solution. For the rigid photodetector, the solution with P3HT and CdSe NWs was dropped on a SiO_2 (300 nm)/Si wafer; then, silver paste was coated on the hybrid film with a spacing of 1 mm. The photodevice was dried at 140 °C in a vacuum oven for 2 h to firm the silver paste. For comparison, photodetectors based on pure CdSe NW film and P3HT film were also fabricated. The flexible photodetectors were constructed on both PET and printing paper by using a similar fabrication process as for the rigid photodetector.

Photoresponse Measurements: The white-light source used was a solar simulator. The incident power of the white light was measured using an Ophir NOVA power meter. Monochromatic light from a source composed of a tungsten lamp (150 W) and a monochromator (WDG15-Z) was focused and guided onto the films. The photocurrent, the dark conductance, and the photoresponse of the photodevices based on P3HT, the CdSe NW film and the P3HT: CdSe NW hybrid film were all recorded using an Autolab (model AUT84315). All of the measurements were performed in air and at room temperature.

Supporting Information

Supporting Information is available from the Wiley Online Library or from the author.

Acknowledgements

X.F.W. and W.F.S. contributed equally to this work.This work was supported by the National Natural Science Foundation (51002059, 21001046, 91123008), the 973 Program of China (2011CBA00703, 2011CB933300), the Program for New Century Excellent Talents of the University in China (grant no. NCET-11-0179), the Research Fund for the Doctoral Program of Higher Education (20100142120053), and the Natural Science Foundation of Hubei Province (2011CDB035). Special thanks to the Analytical and Testing Center of HUST and the Center of Micro-Fabrication and Characterization (CMFC) of WNLO for using their facilities.

Received: June 30, 2012
Revised: August 25, 2012
Published online: October 2, 2012

[1] G. Konstantatos, E. H. Sargent, *Nat. Nanotechnol.* **2010**, *5*, 391.
[2] X. S. Fang, Y. Bando, M. Y. Liao, T. Y. Zhai, U. K. Gautam, L. Li, Y. Koide, D. Golberg, *Adv. Funct. Mater.* **2010**, *20*, 500.
[3] Z. Y. Fan, J. C. Ho, T. Takahashi, R. Yerushalmi, K. Takei, A. C. Ford, Y.-L. Chueh, A. Javey, *Adv. Mater.* **2009**, *21*, 3730.
[4] L. Li, X. S. Fang, T. Y. Zhai, M. Y. Liao, U. K. Gautam, X. C. Wu, Y. S. Koide, Y. Bando, D. Golberg, *Adv. Mater.* **2010**, *22*, 4151.
[5] J. S. Jie, W. J. Zhang, Y. Jiang, X. M. Meng, Y. Q. Li, S. T. Lee, *Nano Lett.* **2006**, *6*, 1887.
[6] Y. Jiang, W. J. Zhang, J. S. Jie, X. M. Meng, X. Fan, S. T. Lee, *Adv. Funct. Mater.* **2007**, *17*, 1795.
[7] X. F. Wang, Z. Xie, H. T. Huang, Z. Liu, D. Chen, G. Z. Shen, *J. Mater. Chem.* **2012**, *22*, 6845.
[8] Y. Ye, L. Dai, X. N. Wen, P. C. Wu, R. Pen, G. G. Qin, *Appl. Mater. Interfaces* **2010**, *2*, 2724.
[9] T. Y. Zhai, X. S. Fang, M. Y. Liao, X. J. Xu, L. Li, B. D. Liu, Y. Koide, Y. Ma, J. N. Yao, Y. Bando, D. Golberg, *ACS Nano* **2010**, *4*, 1596.
[10] H. Chen, L. F. Hu, X. S. Fang, L. M. Wu, *Adv. Funct. Mater.* **2012**, *22*, 1229.
[11] D. Chen, J. Xu, B. Liang, X. F. Wang, P. C. Chen, C. W. Zhou, G. Z. Shen, *J. Mater. Chem.* **2011**, *21*, 17236.

[12] Q. Tang, L. Li, Y. Song, Y. Liu, H. Li, W. Xu, W. Hu, D. Zhu, *Adv. Mater.* **2007**, *19*, 2624.
[13] G. Sarasqueta, K. R. Choudhury, J. Subbiah, F. So, *Adv. Funct. Mater.* **2011**, *21*, 167.
[14] J. J. Wang, Y. Q. Wang, F. F. Cao, Y. G. Guo, L. J. Wan, *J. Am. Chem. Soc.* **2010**, *132*, 12218.
[15] D. J. Xue, J. J. Wang, Y. Q. Wang, S. Xin, Y. G. Guo, L. J. Wan, *Adv. Mater.* **2011**, *23*, 3704.
[16] W. U. Huynh, J. J. Dittmer, A. P. Alivisatos, *Science* **2002**, *295*, 2425.
[17] E. Arici, H. Hoppe, F. Schaffler, D. Meissner, M. A. Malik, N. S. Sariciftci, *Thin Solid Films* **2004**, *451*, 612.
[18] S. Gunes, N. S. Sariciftci, *Inorg. Chim. Acta* **2008**, *361*, 581.
[19] Y. G. Han, G. Wu, M. Wang, H. Z. Chen, *Polymer* **2010**, *51*, 3736.
[20] H. Y. Yang, D. I. Son, T. W. Kim, J. M. Lee, W. II. Park, *Org. Electron.* **2010**, *11*, 1313.
[21] J. J. Wang, J. S. Hu, Y. G. Guo, L. J. Wan, *NPG Asia Mater.* **2012**, *4*, e2.
[22] C. Y. Zhang, X. J. Zhang, X. H. Zhang, X. M. Ou, W. F. Zhang, J. S. Jie, J. C. Chang, C. S. Lee, S. T. Lee, *Adv. Mater.* **2009**, *21*, 4172.
[23] X. F. Duan, *MRS Bull.* **2007**, *32*, 134.
[24] P. C. Chen, G. Z. Shen, H. Chen, Y. Shi, C. W. Zhou, *ACS Nano* **2010**, *4*, 4404.
[25] Z. R. Wang, H. Wang, B. Liu, W. Z. Qiu, J. Zhang, S. H. Ran, H. T. Huang, J. Xu, H.W. Han, D. Chen, G. Z Shen, *ACS Nano* **2011**, *5*, 8412.
[26] B. Liu, J. Zhang, X. F. Wang, G. Chen, D. Chen, C. W. Zhou, G. Z Shen, *Nano Lett.* **2012**, *12*(6), 3005.
[27] R. F. Service, *Science* **2006**, *312*, 1593.
[28] Y. G. Sun, H. H. Wang, *Adv. Mater.* **2007**, *19*, 2818.
[29] S. Holdcroft, *Macromolecules* **1991**, *24*, 4834.
[30] J. F. Wang, M. S. Gudiksen, X. F. Duan, Y. Cui, C. M. Lieber, *Science* **2001**, *293*, 1455.
[31] Q. H. Xiong, J. Wang, P. C. Eklund, *Nano Lett.* **2006**, *6*, 2736.
[32] H. J. Fan, W. Lee, R. Hauschild, M. Alexe, G. L. Rhun, R. Scholz, A. Dadgar, K. Nielsch, H. Kalt, A. Krost, M. Zacharias, U. Gosele, *Small* **2006**, *2*, 561.
[33] V. Sukhovatkin, S. Hinds, L. Brzozowski, E. H. Sargent, *Science* **2009**, *324*, 1542.
[34] C. Soci, A. Zhang, B. Xiang, S. A. Dayeh, D. P. R. Aplin, J. Park, X. Y. Bao, Y. H. Lo, D. Wang, *Nano Lett.* **2007**, *7*, 1003.
[35] Z. Li, O. Kurtulus, N. Fu, Z. Wang, A. Kornowski, U. Pietsch, A. Mews, *Adv. Funct. Mater.* **2009**, *19*, 3650.
[36] D. Chen, J. Xu, B. Liang, X. F. Wang, P.C. Chen, C. W. Zhou, G. Z. Shen, *J. Mater. Chem.* **2011**, *21*, 17236.
[37] G. Z. Shen, B. Liang, X. F. Wang, H. T. Huang, D. Chen, Z. L. Wang, *ACS Nano* **2011**, *5*, 6148.
[38] J. G. Matthew, N. D. Saptapar, H. W. David, E. B. Stephen, L. B. Richard, *ACS Nano* **2012**, *6*, 4222.
[39] H. F. Zhu, T. Li, Y. J. Zhang, H. L. Dong, J. S. Song, H. P. Zhao, Z. M. Wei, W. Xu, W. P. Hu, Z. S. Bo, *Adv. Mater.* **2010**, *22*, 1645.
[40] C. Soci, A. Zhang, B. Xiang, S. A. Dayeh, D. P. R. Aplin, J. Park, X. Y. Bao, Y. H. Lo, D. Wang, *Nano Lett.* **2007**, *7*, 1003.
[41] W. U. Huynh, J. J. Dittmer, A. P. Alivisatos, *Science* **2002**, *295*, 2425.
[42] M. C. McAlpine, H. Ahmad, D. W. Wang, J. R. Heath, *Nat. Mater.* **2007**, *6*, 379.
[43] J. Zhou, Y. D. Gu, Y. F. Hu, W. J. Mai, P. H. Yeh, G. Bao, A. K. Sood, D. L. Polla, Z. L. Wang, *Appl. Phys. Lett.* **2009**, *94*, 191103.
[44] H. Kind, H. Q. Yan, B. Messer, M. Law, P. D. Yang, *Adv. Mater.* **2002**, *14*, 158.
[45] L. F. Hu, L. M. Wu, M. Y. Liao, X. S. Fang, *Adv. Mater.* **2011**, *23*, 1988.